The Journal of Chemical Physics

Band structure for an sp^3 liquid in the single superchain/effective medium approximation

Cite as: J. Chem. Phys. **105**, 7735 (1996); https://doi.org/10.1063/1.472556
Submitted: 14 May 1996 . Accepted: 26 July 1996 . Published Online: 31 August 1998

E. Lomba, J. L. López-Martín, and G. Kahl

Band structure for an sp^3 liquid in the single superchain/effective medium approximation

E. Lomba and J. L. López-Martín
Instituto de Química Física Rocasolano, CSIC, Serrano 119, E-28006 Madrid, Spain

G. Kahl
Institut für Theoretische Physik, Technische Universität Wien, Wiedner Hauptstrasse 8-10, A-1040 Wien, Austria

(Received 14 May 1996; accepted 26 July 1996)

We present a single superchain/effective medium approximation calculation of the electronic density of states for an sp^3 fluid in a tight-binding Hamiltonian approximation, with parameters roughly chosen to represent liquid Hg. Comparison with direct diagonalization of the Hamiltonian using quenched liquid configurations generated by molecular dynamics shows that the performance of the theory is more than acceptable for moderate to high densities. Localization is estimated from the inverse participation ratio calculated from the simulation an in a second order renormalized perturbation theory proposed by Winn and Logan. Analysis of the results indicate that by increasing density the metal nonmetal transition occurs well after the band crossing transition. The major weakness of the theory as far as the density of states is concerned can very likely be coped with by inclusion of nonlinear corrections. © *1996 American Institute of Physics.* [S0021-9606(96)52041-6]

I. INTRODUCTION

The electronic density of states (DoS) or band structure of liquids and amorphous materials has been the focus of interest of a number of recent works[1–8] that use as starting point liquid state theory, vs. the more traditional approach from solid state physics.[9] With a few exceptions[6,8,10] the systems of interest have been studied to the level of linear approximations like the mean spherical approximation[2] or the closely related single superchain/effective medium approximation (SSCA/EMA).[3] Two of the authors have actually taken advantage of the simple formulation of this latter approach to develop a fast and stable algorithm for its numerical solution, that has been successfully tested for an extension of the SSCA/EMA to mixtures of one-band fluids and for two-band fluids.[7] Yet, to our knowledge, most of the systems dealt with hitherto are far from being representative of materials of interest, in particular as regards electronic properties. In this connection, we must recall that the formalism employed is particularly suited to deal with systems where the electronic degrees of fluids can be approximated in terms of tight binding (TB) Hamiltonians,[3] which typically should include at least s and p-bands. In this regard, we are only aware of Chen and Stratt's work[11] on a liquid state theoretical approach for the sp^3 problem. These authors, however, neglect the $s-p$ band interaction. On a more elementary level, Winn and Logan[12] used the Hubbard DoS (which is the low-density limit of other linear theories) for a complete treatment of the localization and DoS of a somewhat naïve model for liquid Hg (Ref. 13) which fully includes the treatment of sp^3 bands with cross interaction present. This work and Chen and Stratt's paper have inspired us to go beyond the Hubbard DoS approach and use the full capabilities of the SSCA/EMA on this problem. For the sake of comparison we have chosen the aforementioned simple model, and hence we do not pretend to attain here a quantitative description of the properties of real Hg.

In addition to the inclusion of cross-interactions, one might argue that the effects of non-orthogonality in the basis functions of the TB Hamiltonian must also be accounted for, but it is also clear that such effects can actually be built-in in the parameterization of the model without further complications. Therefore, the issue of the non-orthogonality is not to be pursued here any further, although its inclusion in the SSCA/EMA formalism is rather straightforward.[11]

A particular feature made apparent in Refs. 10 and 11 is the formal similarity between the p^3-band problem and that posed in liquid theory by determination of the structure of fluids with dipole-dipole interactions. We will see that this similarity can be carried further by establishing a corresponding link between the sp^3 TB band problem and the solution of the Ornstein-Zernike (OZ) equation for the charge-dipole mixture (restricted primitive model of electrolytes), which was solved analytically by Blum[14,15] in the mean spherical approximation (MSA). We will see that following the ideas of Chen and Stratt it is actually simple to recast the SSCA/EMA multi-band equations of Winn and Logan[5] when written for the sp^3 problem in a form that closely resembles (and hence can be handled by the same procedures) the aforementioned ion-dipole statistical mechanical problem. As shown in Ref. 7 the SSCA/EMA equations are particularly suitable for numerical treatment, and thus it is possible to go beyond the limitations of pure analytical solutions, which are only attainable for specific functional forms of the TB transfer matrix elements, such as Yukawa-type interactions and in the MSA. Work on the latter for a Yukawa-type sp^3 is in progress.[16]

In this paper we have thus focused on the numerical solution of the SSCA/EMA equations for a simple sp^3 TB

Hamiltonian which might give a rough approximation to the properties of liquid Hg. Future work will deal with the introduction of non-linear corrections[17] and will concentrate on empirical tight-binding models.[18] Also, our SSCA/EMA calculations have been compared with the result of direct diagonalization of the TB Hamiltonian along a number of configurations independently generated by standard NVE molecular dynamics, in accordance with a quenched liquid picture where the electronic structure depends only parametrically on the atomic positions, and the feedback between the DoS and the spatial correlations of particles is neglected. A more realistic approach should include the self-consistent determination of the dispersion forces from the electronic structure, which as shown by Winn and Kahl[19] is perfectly feasible within the context of the SSCA/EMA approach. Work on this line is in progress. We find that theory and simulation agree remarkably well, already within the linear approximation. Additionally, following the ideas of Winn and Logan[12] who generalized the theory of Abou-Chacra, Anderson and Thouless[20] to multiband models, we have obtained an estimate of the mobility edges, to get a better insight in localization and the influence of band-crossing on the conductivity properties of our model for liquid Hg. Again, as pointed out by Winn and Logan, this only serves to illustrate the uses of the theory within the boundaries of applicability of this somewhat simplistic TB Hamiltonian, bearing in mind that a proper treatment of Hg should go beyond the independent electron approximation.[12,21] On the other hand, additional qualitative information on the localization of the electronic wave functions can also be extracted from the simulation, following the inverse participation ratio (IPR) criterion,[22] which although somewhat inconclusive due to the vague definition of the IPR cutoff (see Ref. 23 for a discussion on this issue) provides interesting information on the presence of localized and extended states in the simulated sample. When comparing the two approaches, we will see that the information provided by the simulations is in *qualitative* agreement with the theoretical predictions which indicate that the metal-nonmetal transition occurs for densities higher than the band-crossing transition density in agreement with the conclusions drawn by Winn and Logan using a Hubbard (semicircular) DoS.

The rest of the paper is organized as follows. In the next section we define the tight binding Hamiltonian which will be the subject of our study. A brief description of the effective liquid metal potential (based on pseudopotential theory) used to model the spatial distribution of atoms in liquid Hg is also included. In Section III we present a brief description of the multi-band SSCA/EMA theory. Expressions are then reformulated and particularized for the sp^3 band model, which is characterized for Hg by the triple degeneracy of the p levels and the angular dependence of the Hamiltonian. A brief account on the two methods to analyze the localization problem is also included here. Details on the simulation procedure and the most significant results and conclusions are presented in Section IV.

II. THE MODEL: sp^3 TB HAMILTONIAN AND EFFECTIVE INTERIONIC POTENTIAL FOR LIQUID Hg

The problem to be addressed concerns the calculation of the distribution of energy levels in a disordered medium, in which the electronic degrees of freedom are governed by a TB Hamiltonian of the form

$$H=\sum_{i,\alpha}\varepsilon_i^{\alpha}a_{i\alpha}^{\dagger}a_{i\alpha}+\sum_{i\neq j,\alpha,\beta}V_{ij}^{\alpha\beta}a_{i\alpha}^{\dagger}a_{j\beta}, \tag{2.1}$$

where the indices i and j run over particle positions (sites) and α,β run over the electronic levels (s and p basis functions in the present instance) located in each site. $a_{i\alpha}^{\dagger}$ ($a_{i\alpha}$) is the creation (annihilation) operator for the state α on site i. The $\varepsilon_i^{\alpha}=\varepsilon_{\alpha}$ since we will restrict ourselves to a case of off-diagonal disorder (ODD). Different ε_i^{α} per site will introduce site diagonal disorder (SDD) which is crucial in modeling the effects of impurities and alloys. In the Hamiltonian (2.1) we have considered a two-center approximation, i.e. crystal field and three center integrals have been neglected for the sake of simplicity. In any case, as mentioned before, these simplifications as well as the neglect of nonorthogonality of the basis functions can be implicitly corrected in the fitting of the parameters of the empirical tight binding model. Finally $V_{ij}^{\alpha\beta}$ are the transfer matrix elements defined by the two center integral

$$V_{ij}^{\alpha\beta}(\mathbf{r}_{ij})=-\int d\mathbf{r}\phi^{\alpha *}(\mathbf{r}-\mathbf{r}_i)\frac{e^2}{|\mathbf{r}-\mathbf{r}_i|}\phi^{\beta}(\mathbf{r}-\mathbf{r}_j), \tag{2.2}$$

where $\phi^{\alpha}(\mathbf{r}-\mathbf{r}_j)$ is the basis wave function centered on site j and e is the electron charge. The full Hamiltonian can be separated into intra- and interatomic components

$$H=\sum_{i\neq j}H_{ij}+\sum_i H_{ii} \tag{2.3}$$

which in terms of sp basis functions read

$$\begin{aligned}H_{ij}&=V^{ss}(r_{ij})a_{is}^{\dagger}a_{js}+\sum_{\mu=x,y,z}V^{p_\mu s}(\mathbf{r}_{ij})a_{ip_\mu}^{\dagger}a_{js}\\&\quad+V^{sp_\mu}(\mathbf{r}_{ij})a_{is}^{\dagger}a_{jp_\mu}+\sum_{\mu,\nu=x,y,z}V^{p_\mu p_\nu}(\mathbf{r}_{ij})a_{ip_\mu}^{\dagger}a_{jp_\nu},\\H_{ii}&=\varepsilon_s a_{is}^{\dagger}a_{is}+\varepsilon_p\sum_{\mu=x,y,z}a_{ip_\mu}^{\dagger}a_{ip_\mu}.\end{aligned} \tag{2.4}$$

Using vector and tensor notation we can rewrite the expression above reorganizing the transfer matrix elements into longitudinal (σ) and transversal (π) components,[24] such that

$$\begin{aligned}H_{ij}&=V^{ss}a_{is}^{\dagger}a_{js}+V_{\sigma}^{sp}a_{is}^{\dagger}\mathbf{a}_{jp}\hat{\mathbf{r}}+V_{\sigma}^{ps}\hat{\mathbf{r}}\mathbf{a}_{ip}a_{js}^{\dagger}+V_{\pi}^{pp}(\mathbf{a}_{ip}^{\dagger}\mathbf{a}_{jp})\\&\quad+[V_{\sigma}^{pp}-V_{\pi}^{pp}(r_{ij})](\mathbf{a}_{ip}^{\dagger}\hat{\mathbf{r}})(\hat{\mathbf{r}}\mathbf{a}_{jp})=V^{ss}(r_{ij})a_{is}^{\dagger}a_{js}\\&\quad+a_{is}^{\dagger}\mathbf{V}_{\sigma}^{sp}(\mathbf{r}_{ij})\mathbf{a}_{jp}+\mathbf{a}_{ip}\mathbf{V}_{\sigma}^{ps}(\mathbf{r}_{ij})a_{js}+\mathbf{a}_{ip}^{\dagger}\mathbf{V}_{\pi}^{pp}(\mathbf{r}_{ij})\mathbf{a}_{jp},\end{aligned} \tag{2.5}$$

where

$$\mathbf{V}_{\sigma}^{sp}(\mathbf{r}_{ij})=V_{\sigma}^{sp}(r_{ij})\hat{\mathbf{r}},$$

$$\mathbf{V}_{\sigma}^{ps}(\mathbf{r}_{ij})=\hat{\mathbf{r}}V_{\sigma}^{ps}(r_{ij}),$$
$$\mathbf{V}^{pp}(\mathbf{r}_{ij})=V_{\pi}^{pp}(r_{ij})\mathbf{I}+[V_{\sigma}^{pp}-V_{\pi}^{pp}(r_{ij})]\hat{\mathbf{r}}\hat{\mathbf{r}}, \tag{2.6}$$

with $\hat{\mathbf{r}}=\mathbf{r}_{ij}/|\mathbf{r}_{ij}|$ and $\mathbf{I}$ is the unit tensor. In the expressions above the creation and annihilation operators have also been written in vector notation. One can see, that after some reordering the pp-term could be rewritten as a linear combination of the dipole-dipole tensor

$$\mathbf{T}(\hat{\mathbf{r}})=3\hat{\mathbf{r}}\hat{\mathbf{r}}-\mathbf{I} \tag{2.7}$$

and the identity matrix $\mathbf{I}$. These quantities are directly related with the angular dependence of the screened dipole-dipole interaction, which is also given by a linear combination of two rotational invariants,

$$\phi^{110}(12)=\hat{\mathbf{s}}_1\mathbf{I}\hat{\mathbf{s}}_2,$$
$$\phi^{112}(12)=\hat{\mathbf{s}}_1\mathbf{T}(\hat{\mathbf{r}})\hat{\mathbf{s}}_2, \tag{2.8}$$

where $\hat{\mathbf{s}}_i$ is a unit vector in direction of the dipole on particle i. Note that here $\hat{\mathbf{r}}\hat{\mathbf{r}}$ is a tensor product, i.e. is a 3×3 matrix, whereas the products in Eq. (2.5) are either scalar products or standard matrix-vector products. Also, the sp (ps) term has a similar relation with the charge-dipole (dipole-charge) interaction, whose angular dependence is described by the $\phi^{011}=(\hat{\mathbf{r}}\hat{\mathbf{s}}_1)$ rotational invariant. This again brings up similarities between these two systems, which will be exploited in the following sections. At this point it is also worth mentioning that this TB Hamiltonian is equivalent to a system composed of particles with embedded three-dimensional plus one dimensional Drude oscillators that are coupled (a model for Frenkel excitons).

Back to our specific problem, far from attempting to model a purely empirical TB Hamiltonian, we have chosen the simple parameterization of Yonezawa and Martino[13] for Hg. Consequently, no comparison with experiment will be attempted here and we will restrict ourselves to the comparison theory vs. simulation. As basis functions we will employ the usual Slater type 2s and 2p orbitals for hydrogen-like atoms, by which the transfer matrix elements from Eq. (2.2) turn into

$$V^{ss}=2\epsilon_2(1+R/2-R^2/6+R^3/24)e^{-R/2},$$
$$V_{\sigma}^{pp}=2\epsilon_2(1+R/2-R^3/24)e^{-R/2},$$
$$V_{\pi}^{pp}=2\epsilon_2(1+R/2+R^2/12)e^{-R/2},$$
$$V_{\sigma}^{sp}=-\frac{\epsilon_2}{3}(R+R^2/2-R^3/4)e^{-R/2},$$
$$V_{\sigma}^{ps}=-V_{\sigma}^{sp}, \tag{2.9}$$

where $R=Zr/a^*$, and $\epsilon_2=-Ze^2/8a^*$, being the effective Bohr radius suggested in (Ref. 13) $a^*=0.64$ Å and $Z=2$. Also, we have used $\varepsilon_p-\varepsilon_s=5.304$ eV. As mentioned by Winn and Logan,[12] with this choice one can safely neglect the non-orthogonality of the orbitals.

As to the spatial distribution of the particles in our quenched liquid, given the relative insensitivity of the DoS interaction potential in this picture (see Ref. 19), we will use a simple liquid metal potential which we found reproduces quite well the experimental structure of liquid Hg.[25] This effective interionic potential is defined by[26,27]

$$u(r)=\frac{(Ze)^2}{r}-\frac{1}{(2\pi)^3}\int \tilde{v}_c(q)F(q)\exp(-i\mathbf{qr})d\mathbf{q}, \tag{2.10}$$

where $\hat{v}_c(q)$ is the Fourier transform of Coulomb potential given by

$$\tilde{v}_c(q)=\frac{4\pi(Ze)^2}{q^2} \tag{2.11}$$

and the energy-wave-number characteristic function $F(q)$ is

$$F(q)=\left(1-\frac{1}{\epsilon(q)}\right)\left|\frac{\tilde{v}(q)}{\tilde{v}_c(q)}\right|^2. \tag{2.12}$$

In this expression $\epsilon(q)$ is the dielectric screening function and $\tilde{v}(q)$ is the Fourier transform of the electron-ion pseudopotential. When using Ashcroft's empty core model we have

$$v(r)=\begin{cases}0 & \text{for} \quad r<R_c\\ -\dfrac{Z}{r} & \text{for} \quad r>R_c,\end{cases} \tag{2.13}$$

whose analytic Fourier transform is

$$\tilde{v}(q)=-\frac{4\pi Ze^2}{q^2}\cos qR_c. \tag{2.14}$$

Now, the dielectric screening function is given by

$$\epsilon(q)=1+\frac{(4\pi Ze^2/q^2)\Pi_0(q)}{1-(4\pi Ze^2/q^2)G(q)\Pi_0(q)}. \tag{2.15}$$

$G(q)$ is the local field correction, which in this case is computed using then Ichimaru-Utsumi's fitting formula,[28] and Π_0 is the Lindhard function

$$\Pi_0(q)=\frac{mk_F}{\pi^2\hbar^2}\left(\frac{1}{2}+\frac{4k_F^2-q^2}{8k_Fq}\ln\left|\frac{q+2k_F}{q-2k_F}\right|\right). \tag{2.16}$$

Here m is the electron mass and k_F the Fermi wavenumber. We have used $R_c=0.619$ Å and $k_F=1.37$ Å taken from Ref. 26. With this effective interionic potential we have run several molecular dynamics simulations to generate the spatial distributions of particles for which the Hamiltonian will be diagonalized and its eigenvalue distribution averaged (in this order). Also reference hypernetted chain (RHNC) calculations have been carried out and present an excellent agreement with MD.[29] The pair distribution functions calculated via the RHNC integral equation are shown in Figure 1. These show a qualitative agreement with recent experimental x-ray measurements[25] and present the characteristic behavior of liquid metals, i.e. as density increases mostly the height of the peaks increases whereas the location remains approximately unchanged. This pair distribution functions will be fed into the SSCA/EMA integral equation to provide the required information on spatial correlations, as will be seen below. It should be mentioned here that the temperature enters our formalism only through the pair distribution func-

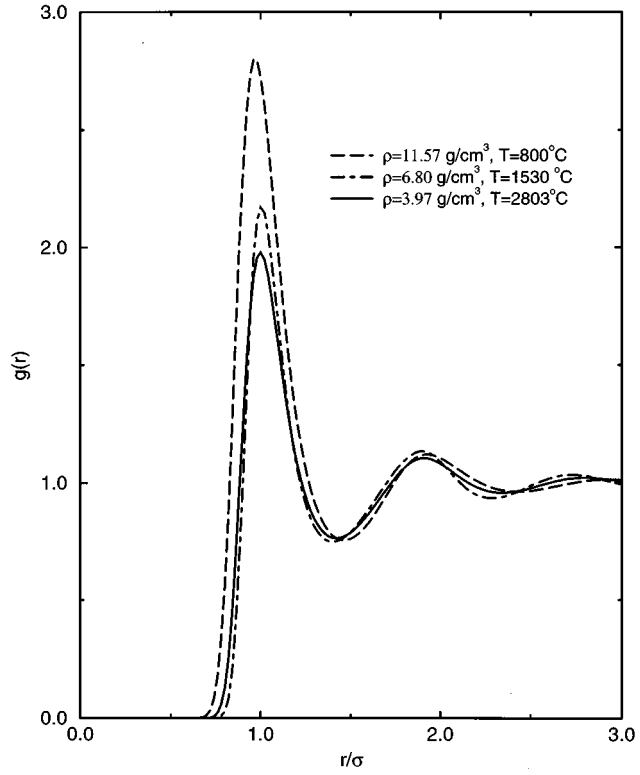

FIG. 1. Pair distribution function for liquid Hg at three thermodynamic states indicated on the legend computed via a RHNC integral equations.

tion, being absent in the zero temperature quantum-mechanical description of the quenched system.

III. SSCA/EMA FORMALISM FOR MULTI-BAND MODELS. APPLICATION TO sp^3 SYSTEMS

In this section we will briefly summarize the essentials of Winn and Logan's treatment of multi-band tight binding models,[5] and the equation will then be cast into a form suitable for the sp^3 band problem, which is somewhat peculiar given its triple degeneracy and its angular dependence.

A. The SSCA/EMA formalism

For a disordered system with a TB Hamiltonian given by Eqs. (2.5) the Green's function for a given configuration fulfills the equation

$$(z-\varepsilon_i^{\alpha})G_{ij}^{\alpha\beta}(z)-\sum_k \sum_{\gamma} V_{ik}^{\alpha\gamma}G_{kj}^{\gamma\beta}(z)=\delta_{ij}\delta_{\alpha\beta}, \qquad (3.1)$$

where $\alpha,\beta=s,p$ and we know that $\mathbf{V}_{ik}^{sp}$ and $\mathbf{V}_{ik}^{pp}$ are a three dimensional vector and a 3×3 matrix respectively. In Eq. (3.1) $z=E+i\epsilon$ ($\epsilon\to0+$). This equation when averaged over ensemble configurations leads to the following expression for the average diagonal Green's function

$$z_{\alpha}\overline{G^{\alpha\beta}}(z)=\delta_{\alpha\beta}+\rho\sum_{\gamma}\int d\mathbf{r}_2 V^{\alpha\gamma}(\mathbf{r}_{12})\overline{G^{\gamma\beta}}(\mathbf{r}_{21}). \qquad (3.2)$$

$\overline{G^{\gamma\beta}}(\mathbf{r}_{21})$ being the average off-diagonal Green's function. Note that now both this quantity and the transfer matrix elements depend on the magnitude and orientation of $\mathbf{r}_{12}$. This equation can be rewritten more compactly in matrix notation

$$\mathbf{z}\overline{\mathbf{G}}=\mathbf{I}+\rho\int d\mathbf{r}_2\mathbf{V}(\mathbf{r}_{12})\overline{\mathbf{G}}(\mathbf{r}_{21}) \qquad (3.3)$$

with $[\mathbf{z}]_{\alpha\beta}=\delta_{\alpha\beta}z_{\alpha}$ ($z_{\alpha}=z-\varepsilon_{\alpha}$) and $V^{11}=V^{ss}$, $V^{12}=\mathbf{V}^{sp}$, and $V^{22}=\mathbf{V}^{pp}$. The same applies to the elements of $\overline{\mathbf{G}}$, but additionally, due to the degeneracy of the p orbitals, $\overline{\mathbf{G}}^{pp}$ is a diagonal matrix with $(\overline{\mathbf{G}}^{pp})_{11}=\overline{G}_{\sigma}^{pp}$, $(\overline{\mathbf{G}}^{pp})_{22}=(\overline{\mathbf{G}}^{pp})_{33}=\overline{G}_{\pi}^{pp}$ (for linear approximation $G_{\sigma}^{pp}=G_{\pi}^{pp}=G^{pp}$) and $\overline{\mathbf{G}}^{sp}=\overline{G}^{sp}(1,0,0)$. Here the coupling of the spherical basis functions with the longitudinal component of the p-band (the one lying along the x-axis as defined here) is understood. The transversal components will always be decoupled. Now one can reorganize the series of the average off-diagonal Green's function following Refs. 5 and 30, and thus express this in terms of its diagonal counterpart as

$$\overline{G}^{\alpha\beta}(\mathbf{r}_{12})=\sum_{\gamma\delta}\overline{G}^{\alpha\gamma}(z)H^{\gamma\delta}(\mathbf{r}_{12})\overline{G}^{\delta\beta}(z), \qquad (3.4)$$

and the spatial dependence is now transferred to a new function $H^{\gamma\delta}(\mathbf{r}_{12})$. This function in turn can be split into sets of diagrams with and without articulation points[3,5] thus defining a function $C^{\gamma\delta}(\mathbf{r}_{12})$ whose constituents resemble those of the direct correlation function in fluid theory, and being $C^{\gamma\delta}(\mathbf{r}_{12})$ and $H^{\gamma\delta}(\mathbf{r}_{12})$ linked by an OZ-like equation

$$H^{\alpha\beta}(\mathbf{r}_{12})=C^{\alpha\beta}(\mathbf{r}_{12})+\rho\sum_{\gamma\delta}\int d\mathbf{r}_3 H^{\alpha\gamma}(\mathbf{r}_{13})\overline{G}^{\gamma\delta}(z)C^{\delta\beta}(\mathbf{r}_{32}). \qquad (3.5)$$

Once again it must be recalled that neither $H^{\alpha\beta}(\mathbf{r}_{12})$ nor $C^{\alpha\beta}(\mathbf{r}_{12})$ are spherically symmetric functions, and consequently some care must be taken to deal with this equation in Fourier space. Equation (3.5) has to be solved in conjunction with a corresponding closure, which in our case will be the SSCA/EMA which reads

$$C^{\alpha\beta}(\mathbf{r}_{12})=g(\mathbf{r}_{12})V^{\alpha\beta}(\mathbf{r}_{12})+(g(\mathbf{r}_{12})-1)\times[H^{\alpha\beta}(\mathbf{r}_{12})-C^{\alpha\beta}(\mathbf{r}_{12})] \qquad (3.6)$$

with $g(\mathbf{r}_{12})$ being the pair distribution function of the fluid.

B. Dealing with the angular dependence: The molecular fluid approach

Due to the nature of our problem, we will have a set of equations in which scalar, vector and matrix functions are combined, except for the closure, which given its linear nature will remain homogeneous. Thus, the OZ equation written explicitly reads

$$H^{ss}=C^{ss}+\rho\int[H^{ss}\overline{G}^{ss}C^{ss}+H^{ss}\overline{\mathbf{G}}^{sp}\mathbf{C}^{ps}+\mathbf{H}^{sp}\overline{\mathbf{G}}^{ps}C^{ss}+\mathbf{H}^{sp}\overline{\mathbf{G}}^{pp}\mathbf{C}^{ps}]d\mathbf{r},$$

$$\mathbf{H}^{sp}=\mathbf{C}^{sp}+\rho\int[H^{ss}\overline{G}^{ss}\mathbf{C}^{sp}+H^{ss}\overline{\mathbf{G}}^{sp}\mathbf{C}^{pp}+\mathbf{H}^{sp}\overline{\mathbf{G}}^{ps}\mathbf{C}^{sp}+\mathbf{H}^{sp}\overline{\mathbf{G}}^{pp}\mathbf{C}^{pp}]d\mathbf{r},$$

$$\mathbf{H}^{ps}=\mathbf{C}^{ps}+\rho\int[\mathbf{H}^{pp}\overline{\mathbf{G}}^{pp}\mathbf{C}^{ps}+\mathbf{H}^{pp}\overline{\mathbf{G}}^{ps}C^{ss}+\mathbf{H}^{ps}\overline{G}^{ss}C^{ss}+\mathbf{H}^{ps}\overline{\mathbf{G}}^{sp}\mathbf{C}^{ps}]d\mathbf{r},$$

$$\mathbf{H}^{pp}=\mathbf{C}^{pp}+\rho\int[\mathbf{H}^{pp}\overline{\mathbf{G}}^{pp}\mathbf{C}^{pp}+\mathbf{H}^{pp}\overline{\mathbf{G}}^{ps}\mathbf{C}^{sp}+\mathbf{H}^{ps}\overline{G}^{ss}\mathbf{C}^{sp}+\mathbf{H}^{ps}\overline{\mathbf{G}}^{sp}\mathbf{C}^{pp}]d\mathbf{r}. \tag{3.7}$$

These equations can be simplified introducing new angular degrees of freedom, so that the quantities that now have dimensionalities higher than one would reduce to scalar quantities with extra angular dependence. In some sense this would be equivalent to consider explicitly the presence of Drude oscillators and averaging over their orientational dependence. These simplifications are possible due to the degeneracy of the p band. Now, we can simply define a new set of angular dependent functions such that

$$H^{sp}(12)=H^{sp}(\mathbf{r}_{12},\omega_2)=\mathbf{H}^{sp}(\mathbf{r}_{12})\hat{\mathbf{s}}_2,$$
$$H^{ps}(12)=H^{sp}(\mathbf{r}_{12},\omega_1)=\hat{\mathbf{s}}_1\mathbf{H}^{ps}(\mathbf{r}_{12}),$$
$$H^{pp}(12)=H^{pp}(\mathbf{r}_{12},\omega_1,\omega_2)=\hat{\mathbf{s}}_1\mathbf{H}^{pp}(\mathbf{r}_{12})\hat{\mathbf{s}}_2, \tag{3.8}$$

where ω_i denotes the Euler angles describing the orientation of the unit vector $\hat{\mathbf{s}}_i$ which has been placed on each site as additional degree of freedom. Similar transformations are needed for the components of $\mathbf{C}$ and $\overline{\mathbf{G}}$. In this latter case the angular functions do not depend on $\omega_{r_{12}}$ and particularly we have $\hat{\mathbf{s}}_1\overline{\mathbf{G}}^{pp}(\mathbf{r}_{12})\hat{\mathbf{s}}_2=\overline{G}^{pp}\hat{\mathbf{s}}_1\hat{\mathbf{s}}_2$. Additionally, we must take into account an important angular convolution property, namely

$$\int(\mathbf{A}\hat{\mathbf{s}}_i)(\hat{\mathbf{s}}_i\mathbf{B})d\omega_i=\frac{1}{3}\mathbf{AB}. \tag{3.9}$$

By using the convolution relation (3.9) and the definitions (3.8), and bearing in mind the *linear nature* of the closure which makes a good number of angular averages vanish, one arrives at the following set of equations

$$H^{ss}(r_{12})=C^{ss}(r_{12})+\rho\int d\omega_3 d\mathbf{r}_3[\overline{G}^{ss}(z)H^{ss}(r_{13})\times C^{ss}(r_{32})+3\overline{G}^{pp}(z)H^{sp}(r_{13},\omega_3)C^{ps}(r_{32},\omega_3)],$$

$$H^{sp}(r_{12},\omega_2)=C^{sp}(r_{12},\omega_2)+\rho\int d\omega_3 d\mathbf{r}_3 3\overline{G}^{pp}(z)\times H^{sp}(r_{13},\omega_3)C^{pp}(r_{32},\omega_3,\omega_2),$$

$$H^{ps}(r_{12},\omega_1)=C^{ps}(r_{12},\omega_1)+\rho\int d\omega_3 d\mathbf{r}_3 3\overline{G}^{pp}(z)\times H^{pp}(r_{13},\omega_1\omega_3)C^{ps}(r_{32},\omega_3),$$

$$H^{pp}(r_{12},\omega_1,\omega_2)=C^{pp}(r_{12},\omega_1,\omega_2)+\rho\int d\omega_3 d\mathbf{r}_3[3\overline{G}^{pp}(z)\times H^{pp}(r_{13},\omega_1\omega_3)C^{pp}(r_{32},\omega_3,\omega_2)+\overline{G}^{ss}H^{ps}(r_{13},\omega_1)C^{sp}(r_{32},\omega_1)]. \tag{3.10}$$

These equations are now formally identical to the equations of an equimolar mixture of charged and dipolar particles, and are appropriate to apply Blum and Torruella's treatment of molecular fluids[31] based on the expansion of the angular functions in rotational invariants

$$F(\mathbf{r}_{12},\omega_1,\omega_2)=\sum_{klm}F^{klm}(r_{12})\phi^{klm}(\omega_1,\omega_2,\omega_{r_{12}}). \tag{3.11}$$

Note that these quantities will appear in the definition of the transfer matrix elements when the transformation (3.8) is applied (see Eq.(2.8)). Expansion (3.11) translates into Fourier space in

$$\tilde{F}(\mathbf{q},\omega_1,\omega_2)=\sum_{klm}\tilde{F}^{klm}(q)\phi^{klm}(\omega_1,\omega_2,\omega_q), \tag{3.12}$$

where the coefficients are given by[31]

$$\tilde{F}^{klm}(q)=4\pi i^m\int_0^\infty r^2F^{klm}(r)j_m(qr)dr \tag{3.13}$$

and conversely

$$F^{klm}(r)=\frac{1}{2\pi^2 i^m}\int_0^\infty q^2\tilde{F}^{klm}(q)j_m(kq)dq \tag{3.14}$$

with $j_m(qr)$ being a spherical Bessel function or order m. Now, it can be shown that if the laboratory reference frame implicit in the expansion (3.11) is changed to an axial reference frame in which the z-axis is located along the line joining the centers, the OZ equation, once deconvoluted in Fourier space and applying the expansion (3.12), will decouple in a set of equations for the expansion coefficients. This change of reference frame translates into the the definition of a new set of coefficients defined with respect to the new reference frame in terms of a spherical harmonic expansion[32]

$$\tilde{F}(\mathbf{q},\omega_1,\omega_2)=\sum_{kl\mu}\tilde{F}_{kl\mu}(q)Y_{k\mu}(\omega_1)Y_{l-\mu}(\omega_2). \tag{3.15}$$

Both sets of coefficients are linked via the following linear combination

$$\tilde{F}_{kl\mu}=\frac{1}{\sqrt{(2k+1)(2l+1)}}\sum_m f^{klm}\begin{pmatrix}k & l & m\\ \mu & -\mu & 0\end{pmatrix}\tilde{F}^{klm} \tag{3.16}$$

and the inverse relation

$$\tilde{F}^{klm}=\sqrt{(2k+1)(2l+1)}\,\frac{2m+1}{f^{klm}}\sum_\mu\begin{pmatrix}k & l & m\\ \mu & -\mu & 0\end{pmatrix}\tilde{F}_{kl\mu} \tag{3.17}$$

with

$$f^{klm}=\frac{l!}{\begin{pmatrix}k & l & m\\ 0 & 0 & 0\end{pmatrix}},$$

where $\begin{pmatrix} k & l & m \\ \mu & -\mu & 0 \end{pmatrix}$ are Wigner's 3-j symbols. These relations obviously hold both in real and Fourier space. Hence once an initial solution is proposed for $\mathbf{H}-\mathbf{C}$, one can compute the rotational invariant projections of the $\mathbf{C}$ matrix from the closure

$$C^{klm}_{\alpha\beta}(r)=g(r)V^{klm}_{\alpha\beta}(r)+(g(r)-1)[H^{klm}_{\alpha\beta}(r)-C^{klm}_{\alpha\beta}(r)], \tag{3.18}$$

which can then be Fourier transformed using Eq. (3.13). Use of Fourier-Bessel transforms of order higher than zero can be avoided using Blum's step-up/step-down procedure.[31,32] Now the spatial coefficients are transformed into axial coefficients by means of Eq. (3.16) which in our particular case reduce to

$$\begin{aligned} F^{sp}_{010}&=F^{011}_{sp}/\sqrt{3},\\ F^{pp}_{110}&=\frac{1}{3}[F^{110}_{pp}+2F^{112}_{pp}],\\ F^{pp}_{111}&=\frac{1}{3}[F^{112}_{pp}-F^{110}_{pp}]. \end{aligned} \tag{3.19}$$

By insertion of the expansion (3.15) into Eq. (3.10) and due to the orthogonality properties of the spherical harmonics, this latter equation decouples into a set of matrix equations,

- $\underline{\mu=0}$

$$\begin{pmatrix} \widetilde{H}^{ss} & \widetilde{H}^{sp}_{010} & \cdots \\ \widetilde{H}^{ps}_{100} & \widetilde{H}^{pp}_{110} & \cdots \\ \cdots & \cdots & \cdots \end{pmatrix} = \begin{pmatrix} \widetilde{C}^{ss} & \widetilde{C}^{sp}_{010} & \cdots \\ \widetilde{C}^{ps}_{100} & \widetilde{C}^{pp}_{110} & \cdots \\ \cdots & \cdots & \cdots \end{pmatrix} + \rho \begin{pmatrix} \widetilde{H}^{ss} & \widetilde{H}^{sp}_{010} & \cdots \\ \widetilde{H}^{ps}_{100} & \widetilde{H}^{pp}_{110} & \cdots \\ \cdots & \cdots & \cdots \end{pmatrix} \times \begin{pmatrix} \overline{G^{ss}} & 0 & \cdots \\ 0 & 3\overline{G^{pp}} & \cdots \\ \cdots & \cdots & \cdots \end{pmatrix} \begin{pmatrix} \widetilde{C}^{ss} & \widetilde{C}^{sp}_{010} & \cdots \\ \widetilde{C}^{ps}_{100} & \widetilde{C}^{pp}_{110} & \cdots \\ \cdots & \cdots & \cdots \end{pmatrix} \tag{3.20}$$

- $\underline{\mu>0}$

$$\widetilde{H}^{pp}_{kl\mu}=\widetilde{C}^{pp}_{kl\mu}+(-1)^{\mu}3\rho\overline{G^{pp}}\sum_{\lambda=\mu}\widetilde{H}^{pp}_{k\lambda\mu}\widetilde{C}^{pp}_{\lambda l\mu}. \tag{3.21}$$

In our particular case only $\mu=1$ is relevant, by which Eq. (3.21) is a scalar equation and Eq. (3.20) is a 2×2 matrix equation. Note that the cross contributions to the Green's function G^{sp} and G^{ps} for linear approximations do not play any role, as was found by Yonezawa and Martino.[13] These equations can be solved for $\widetilde{\mathbf{H}}-\widetilde{\mathbf{C}}$ and a new solution can be generated. It has to be pointed out that to invert the Fourier transform one must proceed stepwise, first obtaining the spatial coefficients using Eq. (3.17) and then invert using the reverse Fourier-Bessel's transform (3.14). Finally, it is worth to write down the explicit expressions for the axial coefficients of the expansion of the transfer matrix elements

$$\begin{aligned} V^{ss}_{000}&=V^{ss},\\ V^{sp}_{010}&=V^{sp}_{\sigma}/\sqrt{3},\\ V^{pp}_{110}&=V^{pp}_{\sigma}/3,\\ V^{pp}_{111}&=V^{pp}_{11-1}=-V^{pp}_{\pi}/3. \end{aligned}$$

We see that the spherical harmonic expansion actually splits the pp interaction into a longitudinal ($\mu=0$, i.e., σ) and two transversal ($\mu=\pm1$, i.e., π) components.

Now we have to apply the same transformations (3.8) and expansions (3.15) to the Green's function equation (3.2) with Eq. (3.4) inserted. One then simply obtains for a linear closure

$$z_s\overline{G^{ss}}=1+4\pi\rho\int[(\overline{G^{ss}})^2V^{ss}(r)H^{ss}(r)-3\overline{G^{pp}}\,\overline{G^{ss}}V^{sp}_{010}(r)H^{ps}_{100}(r)]r^2dr, \tag{3.22a}$$

$$z_s\overline{G^{sp}}=4\pi\rho\int[\overline{G^{ss}}\,\overline{G^{sp}}V^{ss}(r)H^{ss}(r)-3\overline{G^{pp}}\,\overline{G^{sp}}V^{sp}_{010}(r)H^{ps}_{100}(r)]r^2dr, \tag{3.22b}$$

$$z_p\overline{G^{ps}}=4\pi\rho\int[3\overline{G^{pp}}\,\overline{G^{ps}}V^{pp}_{110}(r)H^{pp}_{110}(r)+3\overline{G^{pp}}\,\overline{G^{ps}}V^{pp}_{111}(r)H^{pp}_{111}(r)-\overline{G^{ss}}\,\overline{G^{ps}}V^{ps}_{100}H^{sp}_{010}]r^2dr, \tag{3.22c}$$

$$z_p\overline{G^{pp}}=1+4\pi\rho\int[3(\overline{G^{pp}})^2V^{pp}_{110}(r)H^{pp}_{110}(r)+6(\overline{G^{pp}})^2V^{pp}_{111}(r)H^{pp}_{111}(r)-3\overline{G^{ss}}\,\overline{G^{pp}}V^{ps}_{100}(r)H^{sp}_{010}(r)]r^2dr. \tag{3.22d}$$

Again Eqs. (3.22b) and (3.22c) can only be satisfied if $\overline{G^{sp}}=\overline{G^{ps}}=0$. Now we can define the self-energy in matrix notation[30]

$$\mathbf{S}(z)=\rho\int\mathbf{V}(12)\overline{\mathbf{G}}(z)\mathbf{H}(21)d\mathbf{r}_2 \tag{3.23}$$

by which the average diagonal Green's function is

$$\overline{\mathbf{G}}(z)=[\mathbf{z}-\mathbf{S}(z)]^{-1}. \tag{3.24}$$

The elements of $\overline{\mathbf{G}}$ are then

$$\overline{G^{ss}}(z)=\left[z-\varepsilon_s-4\pi\rho\int[V^{ss}\overline{G^{ss}}(z)H^{ss}-3V^{sp}_{010}\overline{G^{pp}}(z)H^{ps}_{100}]r^2dr\right]^{-1} \tag{3.25}$$

and

$$\overline{G^{pp}}(z)=\Bigg[z-\varepsilon_p-4\pi\rho\int [3V_{110}^{pp}\overline{G^{pp}}(z)H_{110}^{pp} + 6V_{111}^{pp}\overline{G^{pp}}(z)H_{111}^{pp} - V_{100}^{ps}\overline{G^{ss}}(z)H_{010}^{sp}]r^2dr\Bigg]^{-1}, \tag{3.26}$$

where the elements of the **z** matrix are defined below Eq. (3.3). These equations, as indicated in Ref. 7, are numerically very stable and thus will be the ones to which the algorithms proposed in Ref. 7 will be applied. Finally, the total energy density of states of our degenerate multi-band system is given by

$$D(E)=-\lim_{\epsilon\to 0^+}\frac{1}{\pi}[\overline{G^{ss}}(E+i\epsilon)+3\overline{G^{pp}}(E+i\epsilon)]. \tag{3.27}$$

C. Localized and extended states: Simulation and theory

The starting point to deal with the localization issue from a simulation perspective is the diagonalization of the $4N\times 4N$ (N is the number of particles) Hamiltonian matrix, which can be constructed from $N\times N$ submatrices $\mathbf{V}_{ij}$, $i,j=1,\ldots,N$, such that

$$\mathbf{V}_{ij}=\begin{bmatrix} V^{ss} & lV_\sigma^{sp} & mV_\sigma^{sp} & nV_\sigma^{sp} \\ -lV_\sigma^{ps} & l^2(V_\sigma^{pp}-V_\pi^{pp})+V_\pi^{pp} & lm(V_\sigma^{pp}-V_\pi^{pp}) & ln(V_\sigma^{pp}-V_\pi^{pp}) \\ -mV_\sigma^{ps} & ml(V_\sigma^{pp}-V_\pi^{pp}) & m^2(V_\sigma^{pp}-V_\pi^{pp})+V_\pi^{pp} & mn(V_\sigma^{pp}-V_\pi^{pp}) \\ -nV_\sigma^{ps} & nl(V_\sigma^{pp}-V_\pi^{pp}) & nm(V_\sigma^{pp}-V_\pi^{pp}) & n^2(V_\sigma^{pp}-V_\pi^{pp})+V_\pi^{pp} \end{bmatrix}, \tag{3.28}$$

where l,m,n are the x,y,z components of the unit vector $\hat{\mathbf{r}}=\mathbf{r}_{ij}/r_{ij}$ and $i\neq j$. The diagonal submatrices are given by

$$\mathbf{V}_{ii}=\begin{bmatrix} \varepsilon_s & 0 & 0 & 0 \\ 0 & \varepsilon_p & 0 & 0 \\ 0 & 0 & \varepsilon_p & 0 \\ 0 & 0 & 0 & \varepsilon_p \end{bmatrix}.$$

The complete **V** matrix has to be diagonalized for a number of quenched liquid configurations generated according to the interaction potential described in the previous section, and the density of states is obtained from the average of the distribution of eigenvalues using a standard counting procedure. The eigenvectors provide crucial information on the localization of the wave function. The inverse participation ration (IPR) is given by[22]

$$L_r(E_s)=\sum_i^N\left(\sum_\alpha C_{i,r}^\alpha(E_s)^2\right)^2, \tag{3.29}$$

where α runs over the basis functions on each site, i runs over the sites, r designates a given quenched configuration of sites, E_s is the energy eigenvalue and the coefficients of the corresponding normalized eigenfunction are $C_{i,r}^\alpha(E_s)$. If the wave function is fully localized then $L_r=1$ and if completely delocalized then $L_r\to 1/N$ (i.e. for an infinite system $L_r=0$). Gibbons, Logan and Madden[23] used a cutoff value $L_c=K/N=0.16$ (with $K\approx 30-60$) to distinguish between localized and extended states. In any case, there seems to be enough dispute concerning the proper choice of the cutoff value, and therefore we will here simply use the IPR as a *qualitative* indication of the localization of the mobility edges.

As to the theory, Winn and Logan proposed a second order renormalized perturbation approach that leads to very simple expressions once the Green's functions are known.[12] Briefly summarized, the crucial quantity is the eigenvalue

$$\lambda(E)=\{T^{ss}+T^{pp}+2T^{pp'}+[(T^{ss}-T^{pp}-2T^{pp'})^2 + 12T^{sp}T^{ps}]^{1/2}\}/2, \tag{3.30}$$

where p refers to any p_x, p_y or p_z and $p'\neq p$. Then

$$T^{\alpha\beta}(\rho,E)=2\pi[J_1^{\alpha\beta}(\rho)D_\beta(E)]^2/3, \tag{3.31}$$

where

$$D_\beta(E)=-\lim_{\epsilon\to 0^+}\frac{1}{\pi}\overline{G^{\beta\beta}}(E+i\epsilon)$$

and

$$J_1^{\alpha\beta}=\rho\int d\mathbf{r}g(r)|V_{\alpha\beta}(\mathbf{r})|. \tag{3.32}$$

Here $|\cdots|$ denotes the absolute value and $V_{\alpha\beta}$ is the corresponding matrix element of $\mathbf{V}_{ij}$ as defined in Eq. (3.28), i.e. it includes the angular dependence. According to Ref. 12 for a given density ρ, a state corresponding to energy E will be localized if and only if $\lambda<1$ and extended if $\lambda>1$.

IV. RESULTS AND DISCUSSION

The solution of the coupled system of integral equation in complex space presented in the previous section can be handled with the various numerical methods introduced in Ref. 7, and we did not encounter any new difficulties associated with the particular nature of this problem. As to the simulation, we have run a standard NVE simulation for 256 particles, and the DOS and IPR averages were carried out

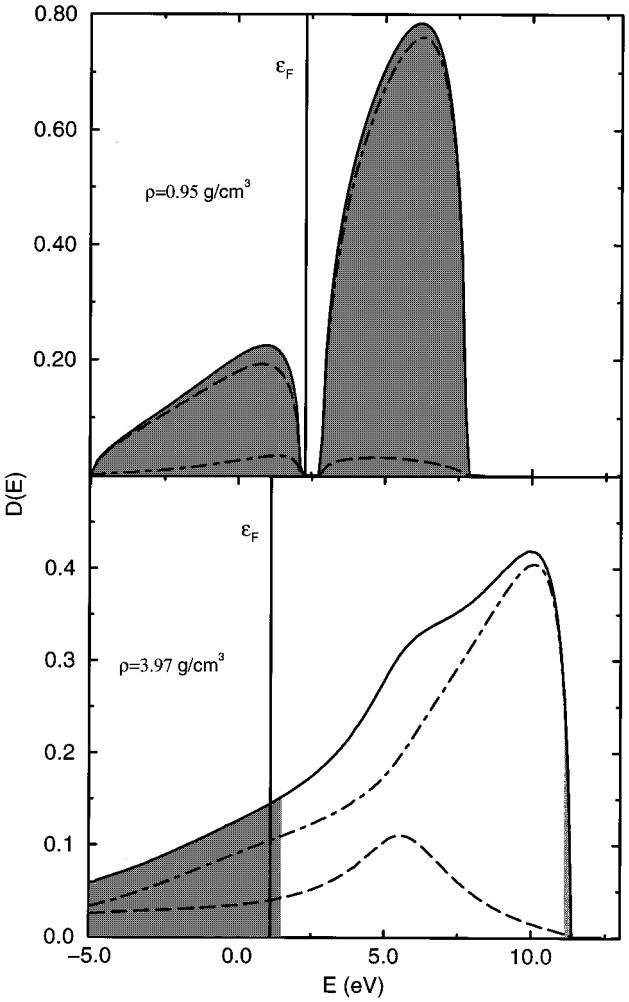

FIG. 2. DoS for liquid Hg at $T=4073$ K and 0.95 g/cm^3 (upper figure) and 3076 K, 3.97 g/cm^3 (lower figure) in the SSCA/EMA. The shaded areas indicate localized states. Dash dotted lines represent the contribution from the p-band and long dashed lines that of the s-band. A vertical line shows the location of the Fermi energy, E_F.

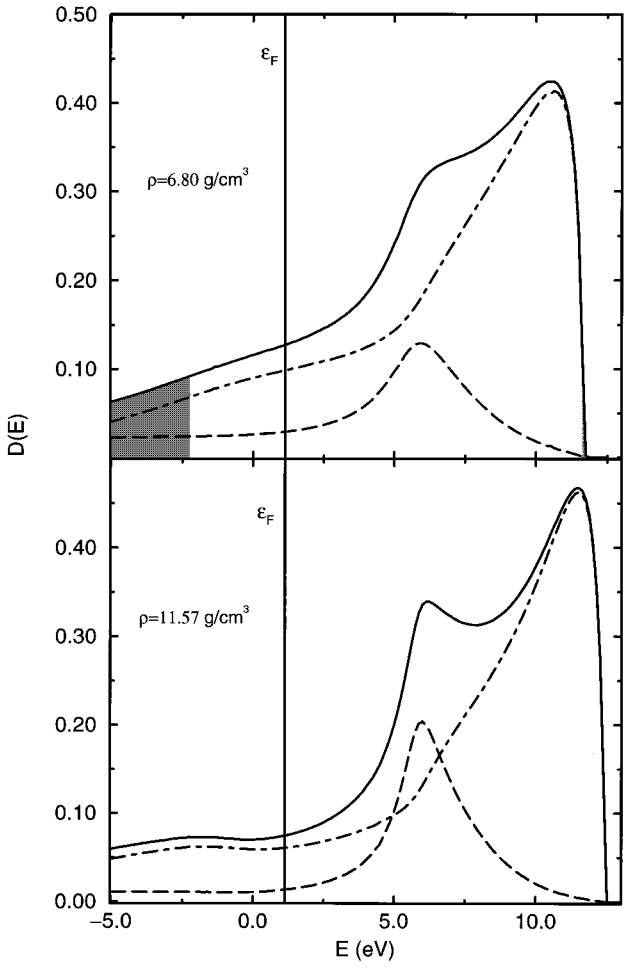

FIG. 3. Same as Figure 2 for $T=1803$ K and 6.80 g/cm^3 (upper figure) and 1073 K, 11.57 g/cm^3 (lower figure).

every 50 MD steps, along a 10000 step run. We have considered four thermodynamics states, 0.95 g/cm^3 ($T=4073$ K), 3.97 g/cm^3 ($T=3076$ K), 6.80 g/cm^3 ($T=1803$ K) and 11.57 g/cm^3 ($T=1073$ K). The choice of these states does not claim to physical relevance (which is also due to the fact that the TB phase diagram might differ from the ''real'' phase diagram) but have rather been chosen for technical reasons. In particular, the first density is artificially low and was used to be able to generate a band gap illustrating the low density behavior of the linear closure and the temperature is sufficiently high to avoid spinodal divergences when calculating the pair distribution function. The second density is close to the state chosen by Winn and Logan.[12] Figures 2 and 3 present the theoretical results with both s and p contributions explicitly indicated. The shaded area denotes the presence of localized states. The Fermi energy has been calculated with the requirement of one fourth of the band filled. It can be appreciated the nearly semicircular band shape (resembling a Hubbard DoS) obtained at very low density, with the Fermi energy lying in the band gap. All the states are localized and consequently the system is insulating, both from the location of the Fermi energy with respect to the band gap and from the localization criterion.

For higher densities (3.97 g/cm^3) the band gap has already disappeared and we can now find evidence of extended states, with a narrow localized region at high energies and a much wider localized region at low energies. It is important to note that the Fermi energy lies within the low energy localized region, and hence this state would be insulating even if we have a partially filled band and there is no band gap. This is in accordance with the findings of Winn and Logan using the Hubbard DoS,[12] although the distribution of localized and extended states (and obviously the shape of the bands except for the very low density) is somewhat different. As the density is further increased the localized states turn less and less important and the system becomes conducting.

Now if one compares the SSCA/EMA results with the computer simulation generated DoS (Figs. 4 and 5), it is possible to appreciate the typical low density departures which stem from the missing two-particle contribution to the DoS in linear theories.[15] At higher densities the results clearly improve (especially for 6.8 g/cm^3), although at $\rho=11.57$ g/cm^3 the s-peak is overestimated. This is also a

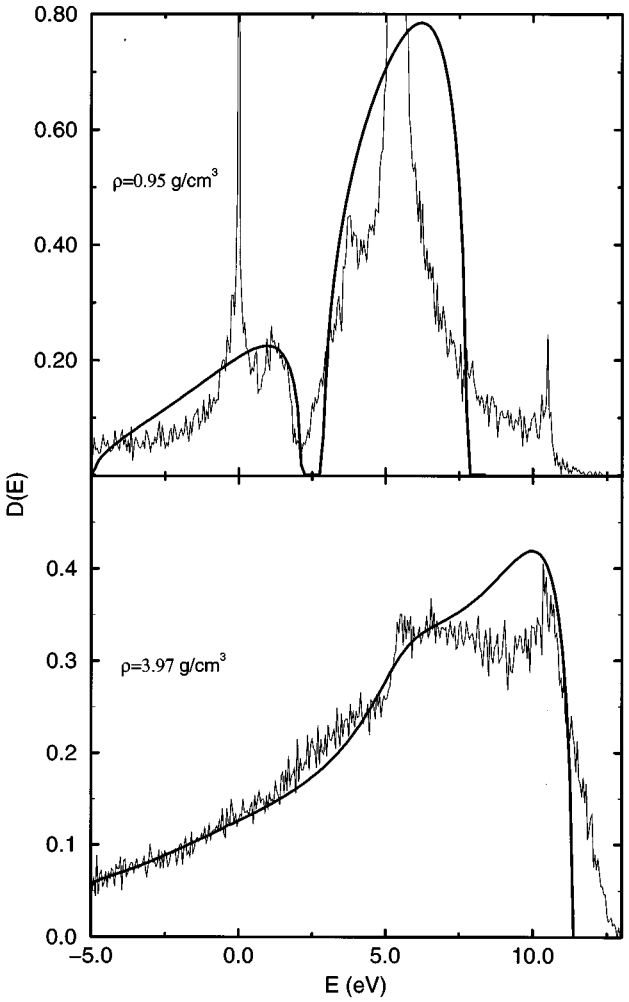

FIG. 4. Simulation (thin lines) vs. SSCA/EMA (thick lines) DoS for liquid Hg at $T=4073$ K and 0.95 g/cm^3 (upper figure) and 3076 K, 3.97 g/cm^3 (lower figure).

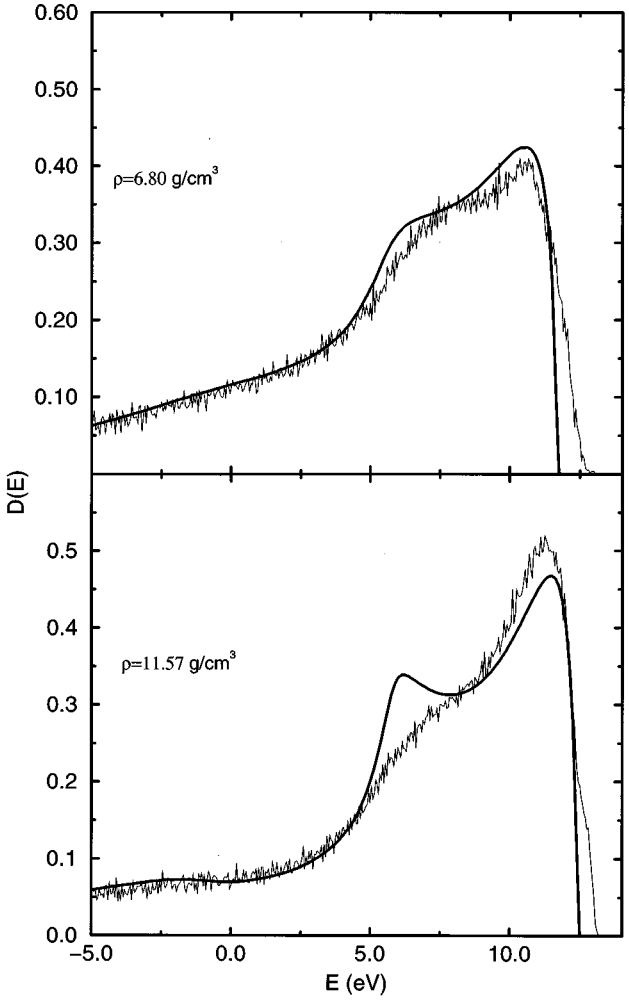

FIG. 5. Same as Figure 4 for $T=1803$ K and 6.80 g/cm^3 (upper figure) and 1073 K, 11.57 g/cm^3 (lower figure).

well known problem of linear approximations which tend to overestimate the heights of the peaks at high densities. Another characteristic shortcoming of the linear approximation is the incorrect treatment of the wings of the spectrum, and this can also be appreciated in Figs. 4 and 5.

As to the information on localization extracted from the simulation this is collected in Figures 6 and 7. We would like to point out discrepancies with the results obtained from the IPR approach. For one thing, and in accordance with Winn and Logan's theory, the very low density state is completely localized. At higher densities however, we see that localized states are expected to appear in the low energy region of the spectrum and in a much narrower area close to the higher energy states. The theoretical prediction for the upper mobility edge is qualitatively correct whereas a large discrepancy is found for the lower mobility edge which is expected to appear at much lower energies according to the IPR criterion. The small peak exhibited by this quantity around 5 eV is probably a remnant of a small localized region very likely present at lower densities, which is predicted at $\rho=4\text{g/cm}^3$ when one uses Hubbard DoS (see Figure 2 in Ref. 12). In our case, this region is expected to appear at lower densities, and that is probably the case both in theory and in simulation. We have not bothered to investigate this further since in the present instance it does not seem crucial for the metal/insulator transition. Finally, for the larger densities, the regions of localized states shrink almost completely, to the point that are hard to detect using the IPR criterion, being the statistics of the significant portions of the IPR much poorer when the number of localized states diminishes. In summary, according to both theory and simulation the metal/insulator transition is induced in this model by localization effects but should occur at densities somewhat lower that those predicted by the theory. It should be pointed out that the theory is susceptible of improvement if the treatment of localization is brought to the same level of approximation as the theoretical DoS.[33]

In summary, we have presented a theory that can actually deal with the problem of the DoS in multi-band sp^3 TB Hamiltonians, to the point that even with the limitations of linear theories gives reasonable results. Non-linear corrections to the SSCA/EMA in the line of work of Høye *et al.*[6,15] are currently under investigation and we expect that these

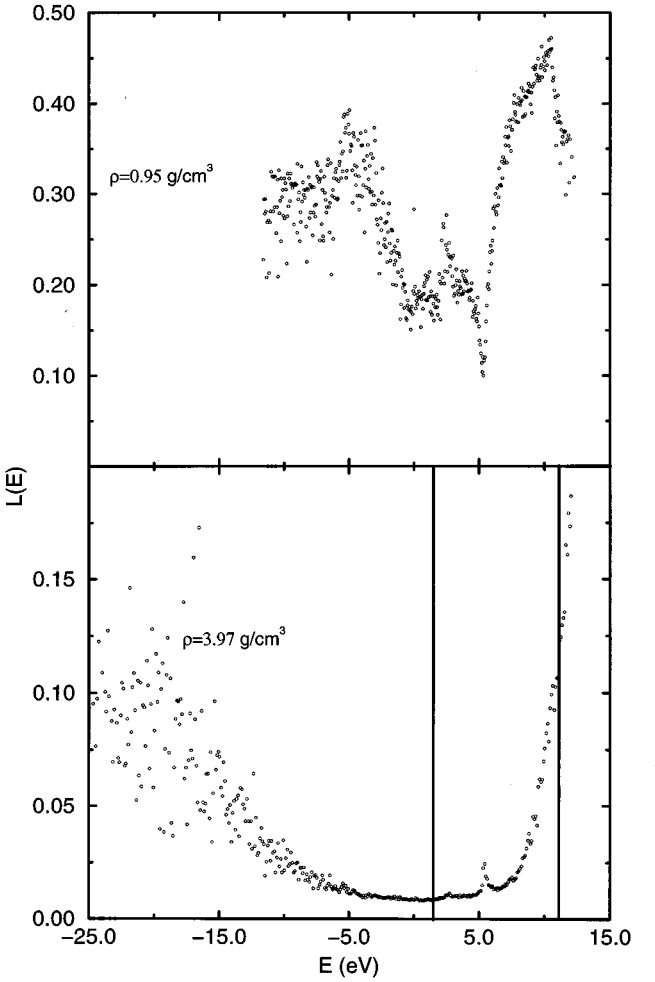

FIG. 6. Average inverse participation ratio (see Eq. (3.29)), L(E) for liquid Hg at $T=4073$ K and 0.95 g/cm^3 (upper figure) and 3076 K, 3.97 g/cm^3 (lower figure). The theoretical mobility edges are shown as vertical lines.

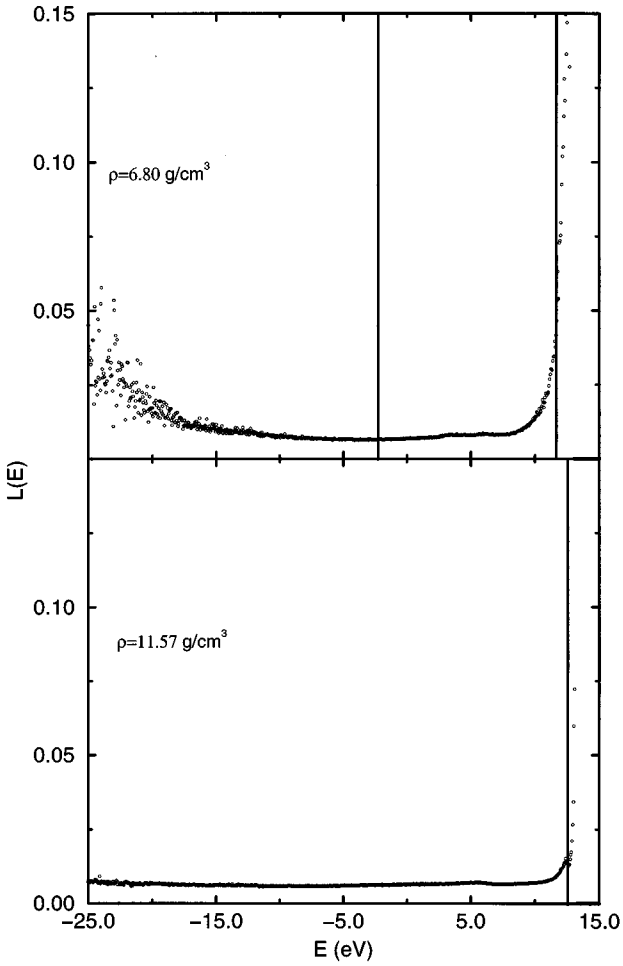

FIG. 7. Same as Figure 6 for $T=1803$ K and 6.80 g/cm^3 (upper figure) and 1073 K, 11.57 g/cm^3 (lower figure). The theoretical mobility edges are shown as vertical lines.

corrections will be essential to treat more realistic TB Hamiltonians which are likely to deviate much more from the mean spherical behavior, given the short range of empirically parameterized interactions.[18] Work on these issues is planned.

ACKNOWLEDGMENTS

The authors are particularly grateful to Professor J.S. Høye for his critical reading of the manuscript and his helpful suggestions. Fruitful discussions with Dr. M.D. Winn are also acknowledged. This research was financially supported by the Spanish Dirección General de Investigación Científica y Técnica (DGICYT) under Grant PB94-0112. The authors wish to acknowledge support from the Austrian-Spanish Program of Acciones integradas under Grant HU1995-0015. E.L. would like to thank the Institut für Theoretische Physik in Vienna for its hospitality during the period when this work was conceived.

[1] R.M. Stratt, Annu. Rev. Phys. Chem. **41**, 175 (1990).
[2] B. Xu and R.M. Stratt, J. Chem. Phys. **91**, 5613 (1989).
[3] D.E. Logan and M.D. Winn, J. Phys. C **21**, 5773 (1988).
[4] M.D. Winn and D.E. Logan, J. Chem. Phys. **96**, 4818, (1992).
[5] M.D. Winn and D.E. Logan, J. Phys. Condensed Matter **1**, 8683 (1989).
[6] J.S. Høye and E. Lomba, J. Chem. Phys. **101**, 4083 (1994); J.S. Høye, E. Lomba, and J.L. López Martín, *ibid.* **101**, 9042 (1994); J.S. Høye, J.L. López Martín, and E. Lomba, *ibid.* **103**, 2178 (1995).
[7] E. Lomba and J.L. López Martín, J. Chem. Phys. **104**, 5244 (1996).
[8] Z. Chen and R.M. Stratt, J. Chem. Phys. **97** , 5687 (1992).
[9] See Chap. 7, in *The Physics of Structurally Disordered Matter*, edited by N.E. Cusack (Adam Hilger, Bristol, 1987).
[10] M.D. Winn and G. Kahl, J. Chem. Phys. **101**, 10850 (1994).
[11] Z. Chen and R.M. Stratt, J. Chem. Phys. **94**, 1426 (1991).
[12] M.D. Winn and D.E. Logan, J. Chem. Phys. **93**, 6756 (1990).
[13] F. Yonezawa and F. Martino, J. Phys. F **6**, 739 (1976).
[14] L. Blum, J. Chem. Phys. **61**, 2129 (1974).
[15] J.S. Høye and E. Lomba, J. Chem. Phys **89**, 7462 (1988).
[16] J.S. Høye and E. Lomba (unpublished).
[17] J.S. Høye, E. Lomba and J.L. López Martín (unpublished).
[18] C.Z. Wang, C.T. Chan, and K.M. Ho, Phys. Rev. B **45**, 2227 (1992); C.Z. Wang, K.M. Ho, and C.T. Chan, *ibid.* **47**, 14835 (1993).
[19] This feedback is however taken into account when a proper tight binding molecular dynamics is performed, through evaluation of the Hellman–Feynmann dispersion forces. Also, an iterative procedure which includes the influence of the DoS on the dispersion forces has recently been proposed in the context of the SSCA/EMA. See, M.D. Winn and G. Kahl, J. Chem. Phys. **100**, 7836 (1994).
[20] R. Abou-Chacra, P.W. Anderson, and D.J. Thouless, J. Phys. C **6**, 1734 (1973).

[21] W. Jank and J. Hafner, Phys. Rev. B **42**, 6926 (1990).
[22] R.J. Bell and P. Dean, Discuss. Faraday. Soc. **50**, 55 (1970).
[23] M.K. Gibbons, D.E. Logan, and P.A. Madden, Phys. Rev. B **38**, 7292 (1988).
[24] J.C. Slater and G.F. Koster, Phys. Rev. A **94**, 1498 (1954).
[25] K. Tamura and S. Hosokawa, J. Non-Cryst. Solids **156–158**, 646 (1993).
[26] J. Hafner, *From Hamiltonians to Phase Diagrams* (Springer, Berlin, 1987).
[27] M. Hasegawa, K. Hoshino, M. Watabe and W.H. Young, J. Non-Cryst. Solids **117 & 118**, 300 (1990).
[28] S. Ichimaru and K. Utsumi, Phys. Rev. B **24**, 7385 (1981).
[29] E. Lomba, M. Alvarez, G. Stell, and J.A. Anta, J. Chem. Phys. **97**, 4349 (1992).
[30] M.S. Wertheim, Mol. Phys. **25**, 211 (1973).
[31] L. Blum and A.J. Torruella, J. Chem. Phys **56**, 303 (1972).
[32] F. Lado, Mol. Phys. **47**, 283 (1982).
[33] M.D. Winn (private communication); see M.D. Winn and D.E. Logan, Phys. Chem. Liquids **22**, 11 (1990) for a complete treatment of the localization problem in the same level of approximation of the EMA for the DoS.